ARTICLE

Direct Compressive Measurements of Individual Titanium Dioxide Nanotubes

Tolou Shokuhfar,[†,§,*] Ganesh K. Arumugam,[‡] Patricia A. Heiden,[‡,§] Reza S. Yassar,[†,§] and Craig Friedrich[†,§]

[†]Department of Mechanical Engineering-Engineering Mechanics, [‡]Department of Chemistry, and [§]Multi-Scale Technologies Institute, Michigan Technological University, Houghton, Michigan 49931

ABSTRACT The mechanical compressive properties of individual thin-wall and thick-wall TiO_2 nanotubes were directly measured for the first time. Nanotubes with outside diameters of 75 and 110 nm and wall thicknesses of 5 and 15 nm, respectively, were axially compressed inside a 400 keV high-resolution transmission electron microscope (TEM) using a new fully integrated TEM—atomic force microscope (AFM) piezo-driven fixture for continuous recording of the force-displacement curves. Individual nanotubes were directly subjected to compressive loading. We found that the Young's modulus of titanium dioxide nanotubes depended on the diameter and wall thickness of the nanotube and is in the range of 23—44 GPa. The thin-wall nanotubes collapsed at ~1.0 to 1.2 μN during axial compression.

KEYWORDS: titanium oxide nanotubes · mechanical properties · *in situ* TEM

TiO_2 is a highly functional material with a wide range of applications that are based on its semiconductive and biocompatible nature. The semiconductive nature makes TiO_2 suitable for water-splitting, photocatalysis, and for self-cleaning applications.[1−3] Biocompatibility is highly important in biology and medicine, where the TiO_2 layers on Ti and Ti alloys are in direct contact with biological tissue in hip or dental implants.[4] For several applications, a nanostructured layer with a high surface area, possibly a uniform distribution, and excellent charge-transfer properties is beneficial for good performance.

Gong and co-workers reported the synthesis of TiO_2 nanotube arrays using an aqueous HF based electrolyte.[5] The pH of F^- ion containing electrolytes was controlled to form nanotubes up to a few micrometers in length. They reported that the tube properties varied dramatically with the electrolyte chemistry in which they were formed. For instance, close-packed hexagonal tubes were formed when using an ethylene glycol electrolyte.[6] Removal of the tube "plug" by an acid rinse enabled fabrication of free-standing, self-supportive membranes that can be used for biofiltration.[7,8] In contrast, tubes formed from dimethyl sulfoxide (DMSO) electrolytes had weak tube-to-tube binding. Further studies focused on precise control and extension of the nanotube morphology,[9] length, pore size,[10] and wall thickness.[11] Various doping strategies have been pursued including the use of an organic anodization bath and incorporation of anionic species during the anodization process.[5,12]

To our knowledge, direct measurements of the compressive mechanical properties of individual TiO_2 nanotubes with *in situ* TEM have not been reported. Only very recently, Crawford *et al.* used nanoindentation to measure the Young's modulus of TiO_2 nanotube films deposited on Ti substrates.[13] The authors reported a significant contribution from the substrate on the force measurements and used the role of mixture for composite materials (weighted sum of modulus-volume fractions of the constituents) to estimate the Young's modulus of the nanotube films. In the present work we performed direct compressive force measurements of titanium dioxide nanotubes inside a 400 keV high-resolution field-emission transmission electron microscope eliminating the prior approximation. A novel integrated AFM−TEM holder equipped with a MEMS force sensor enabled the *in situ* and direct quantitative measurements of the nanotube compressive characteristics. The mechanical tests in the TEM allowed us to not only evaluate the compressive stresses and estimate the elastic modulus of individual TiO_2 nanotubes, but also to moni-

*Address correspondence to tshokuhf@mtu.edu.

Received for review March 1, 2009 and accepted September 8, 2009.

Published online September 23, 2009. 10.1021/nn900202x CCC: $40.75

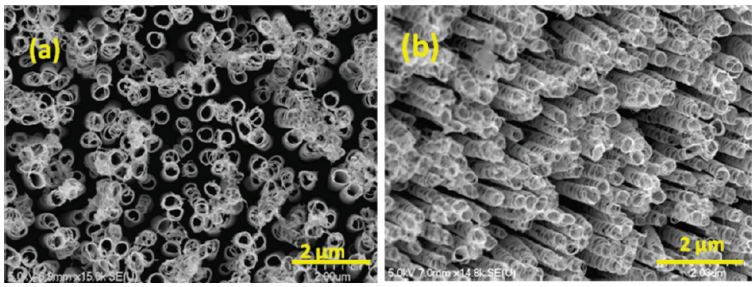

Figure 1. FESEM images of a TiO_2 nanotube array sample etched with a 2.0% HF-DMSO electrolyte for 40 h at 60 V.

tor and dynamically record the tube structural changes during loading.

RESULTS AND DISCUSSION

The anodization resulted in vertically oriented TiO_2 nanotube arrays as shown in Figure 1. Nanotubes had lengths between 7−10 μm and inner diameters ranging from 60−130 nm. The tubes were easily dispersed enabling their use. This allowed us to directly measure the properties of an individual tube and to characterize the compressive behavior.

With respect to the experimental verification of mechanical properties of TiO_2 nanotubes, no direct measurements appear to have been reported. Crawford *et al*. used nanoindentation to probe the mechanical response of TiO_2 nanotube films on a Ti substrate.[13] They proposed that the regions immediately under the indenter tip were subjected to densification, while those at the sides of the indenter were under shear stress that induced both densification and wear of the nanotubes. No direct measurement of force-displacement on a single nanotube was reported; however, the authors did report progressively higher values of the Young's modulus for thinner films of TiO_2 nanotubes consistent with the increased influence of the underlying Ti substrate.

In the present work we performed direct force-displacement measurements during compressive loading of high purity, well-structured individual TiO_2 nanotubes inside a 400 keV high-resolution JEOL TEM. The accuracy and capability of this technique for direct measurements have been discussed in a number of recent publications.[14−20] For instance Golberg *et al*. measured the bending force and modulus of boron nitride nanotubes using an *in situ* AFM-TEM technique.[18] In our work, an AFM cantilever holder equipped with a MEMS force sensor enabled *in situ* and direct measurements of

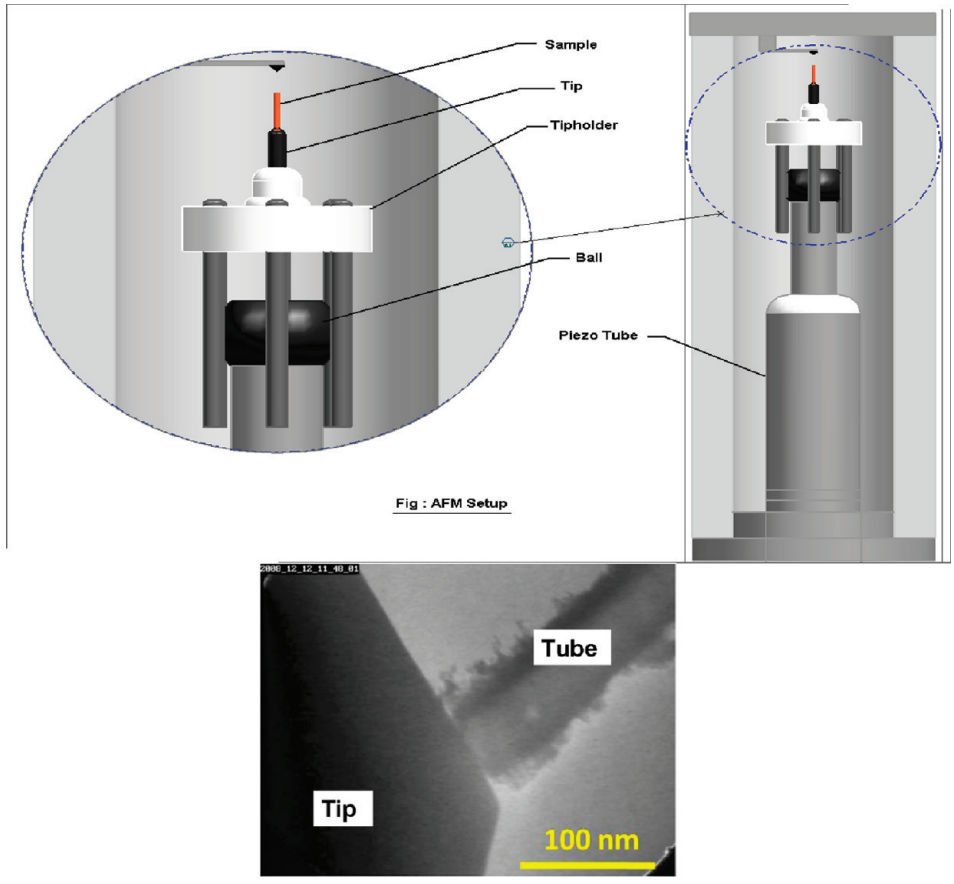

Figure 2. Schematic of the experimental setup within an AFM−TEM holder. The inset on the right shows a TEM view of a titanium dioxide nanotube being compressed between a sample wire and a silicon cantilever. The initial position of the tube against the cantilever may be precisely adjusted with piezo-driven displacement of the sample wire.

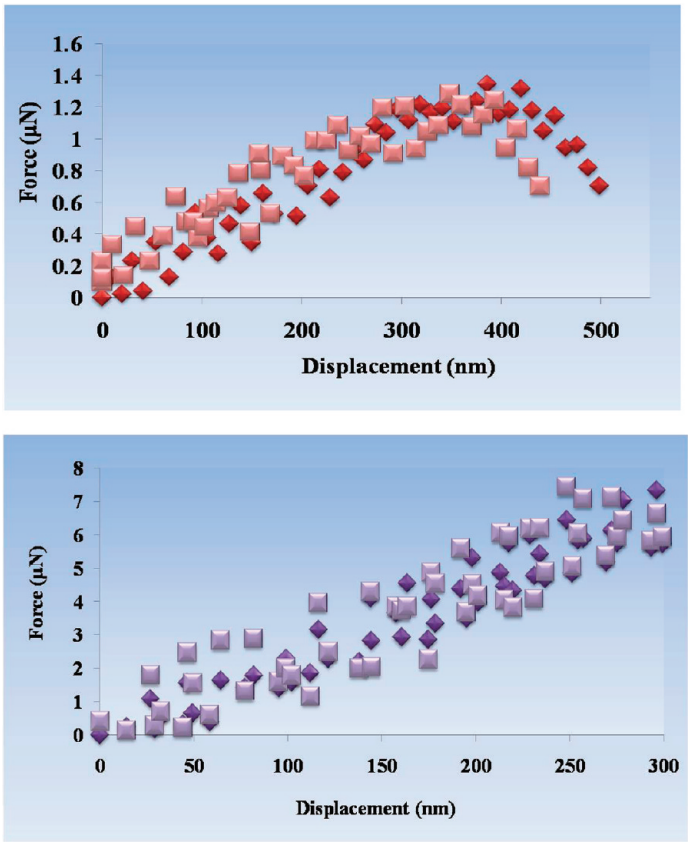

Figure 3. Force *vs* displacement curves recorded for the thin-wall (top) and thick-wall (bottom) TiO_2 nanotubes. The data from multiple experiments for each tube is overlaid in each plot with different color.

the compressive properties of the nanotubes. The experimental setup is shown schematically in Figure 2. A silicon cantilever was attached to a fixed MEMS force sensor and a gold wire with a mounted TiO_2 nanotube was placed on the piezo-movable side of the holder. Initially, the relative positions of the wire and cantilever were manually adjusted with tweezers under an optical microscope to reduce the gap between them. Finally, the *X*, *Y*, and *Z* positions of the cantilever and individual TiO_2 nanotube were adjusted with the precision piezo-driven manipulator of the gold wire. The nanotube motion and force acquisition parameters were controlled by software and electronics from Nanofactory Instruments AB. This automatically coordinated the stages and controlled the TiO_2 nanotube displacement and rate. Prior to nanotube compression, the sensor system was calibrated by indenting a Au wire, and the calibration coefficients were introduced into the sensor system software. During the experiments, we monitored and recorded the compressive force-displacement of the individual TiO_2 nanotubes.

Two representative TiO_2 nanotubes were used for *in situ* TEM measurements, which we refer to as "thin-wall" and "thick-wall". The thin-wall tube had external and internal nominal diameters of ~75 and ~65 nm. The thick-wall tube had external and internal nominal diameters of ~110 and ~80 nm. The typical lengths of tubes prior to compression were 7−10 μm.

The typical force-displacement curves of the thin-wall and thick-wall TiO_2 nanotubes during compression are shown in Figure 3. The compression tests were repeated for several nanotubes to ensure the reproducibility of the data as they are shown with different color in each plot. In general, for Figure 3a and 3b, the maximum observed standard deviations were 0.25 and 0.85 μN, respectively. The maximum applied forces were directly measured to be ~1.2 μN for the thin-wall tube and ~7 μN for the thick-wall tube. By measuring the TiO_2 nanotube internal and external nominal diameters and length in the TEM, we were able to estimate the compressive stresses to be 1091 MPa for the thin-wall tube and 1475 MPa for the thick-wall tube. We refer to the nominal diameter because the cross-section dimensions of a tube were estimated by its two-dimensional projection viewed in the TEM. To calculate the elastic modulus, we used the engineering stress and the engineering strain based on an average tube length of 8.5 μm. We obtained the elastic modulus of the nanotubes to be 23 GPa and 44 GPa for thin-wall and thick-wall tubes, respectively. The calculated elastic modulus data are in close agreement with the Young's modulus values reported by Crawford *et al.* who used nanoindentation.[13] Their reported values were in the range of 36−43 GPa. Our approach is different and provides direct force measurements on a single nanotube. Although the highest elastic modulus that we obtained is similar to that of Crawford *et al.*, we found nanotubes with a lower Young's modulus (23 GPa) than the values reported by these authors (36 GPa).

Moreover, the *in situ* TEM studies allowed us to correlate the load−displacement measurements with changes in the tubes' structure. During compressive loading, a phenomenon was observed that corresponds to the drop of force on the thin-wall tube shown in Figure 3. The correlation of load measurements with TEM images indicated that the thin-wall TiO_2 nanotube exhibited a force-displacement response similar to yielding in a conventional ductile material. A TEM image of a thin-wall nanotube is shown in Figure 4 and the inset shows the collapsed zone which apparently caused the drop in compressive force. The collapse of thin-wall nanotubes could be due to localized deformation and failure originated by nanoscale defects. As seen in the TEM images, the nanotube surface contains irregularities, and this may have caused stress concentration and failure.

The collapse of carbon nanotubes due to compressive loading has been predicted by atomistic simulation. Yokobson *et al.* observed that under axial compression, a carbon nanotube undergoes various atomistic mechanisms.[21] Within the Hookean range of strain, and even at larger strains where the stress−strain relation deviates from linear, they did

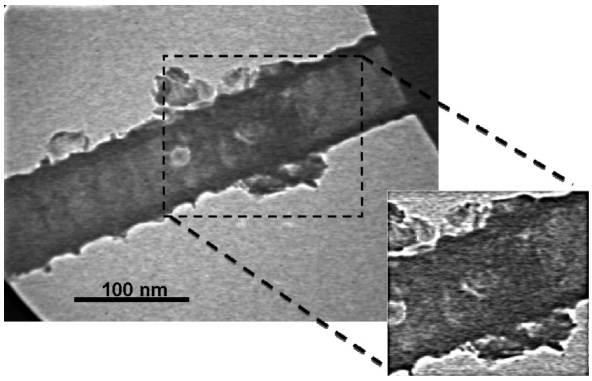

Figure 4. A TiO_2 nanotube fractured after application of maximum compressive load. The inset shows the collapse of the nanotube due to compressive load.

not see any bond switching or breaking in the nanotube. There were no indications of plastic behavior, that is, the formation of dislocation-like defects and their motion within the strained nanotube body. At a certain critical level, which is natural to identify with the breaking strain, one or a few C−C bonds break almost simultaneously, and the resulting "hole" in the tube wall became a precursor of fracture. The atomic disorder propagated very quickly along the circumference of the tube. The strain, which was quite uniform along the tube before this threshold, now redistributed itself to form a largely distorted and unstable neck between the two relaxing nanotube segments.

Using the Euler formula, $\sigma_{cr} = \pi^2 EI/(AL^2)$, where σ_{cr} is the critical stress, E is the elastic modulus, I is the moment of inertia, A is the column cross section, and L is the length of the column, one might expect to observe buckling phenomenon rather than collapse by compression. However, certain conditions need to be met before applying the Euler formula to an axially stressed column. The Euler buckling equation is only valid for long and slender columns loaded axially in compression. What determines this long and slender criterion is the ratio of the effective length (KL) of a column to the least radius of gyration, $r = (I/A)^{0.5}$, of its cross section. Considering a fixed end ($K = 0.5$) scenario, in the case of our TiO_2 nanotubes, this ratio was calculated to be ~120. This value can be categorized in the intermediate range of slender ratios, and buckling failure can happen at higher slender ratios.

The compression experiments inside the TEM allowed us to track the structural changes within an individual deformed nanotube. This is an appealing advantage of the present *in situ* TEM technique over the AFM,[6,9] and SEM-based setups,[21−25] which suffer from insufficient spatial resolution leaving unanswered deformation-related questions about elastic and/or plastic deformation. It is interesting to note that the Young's modulus monotonically decreases with the bulk TiO_2, the thick-wall, and thin-wall nanotube dimensions.

CONCLUSION

Direct force measurements were performed during compressive deformation of individual titanium dioxide nanotubes using an AFM cantilever, piezo-driven holder inside a 400 keV JEOL high-resolution, field-emission transmission electron microscope. The measured forces ranged between 1.2 and 7 μN. These forces, coupled with the observed TiO_2 nanotube dimensions, correspond to compressive stresses up to 1564 MPa and lead to a Young's modulus of TiO_2 nanotubes in the range of 23 to 44 GPa. By taking advantage of the presumed changes in deformation mechanisms within nanocrystalline materials such as the titanium dioxide nanotubes reported here, it is possible that much higher specific strengths can be realized, and structural deformation at the nanoscale can be exploited to make advanced engineering materials.

EXPERIMENTAL SECTION

Titanium foils (250 μm thick, purity ~99.7%, Sigma-Aldrich) were ultrasonically cleaned in acetone and ethanol. The foils were anodized in a two-electrode electrochemical cell in an electrolyte containing dimethyl sulfoxide (DMSO) (99.6%, Aldrich) and hydrofluoric acid (HF, 48% aqueous solution, JT Baker). The anodization voltage, HF concentration in DMSO, and duration of anodization were 60 V, 2 wt %, and 40 h, respectively. Platinum foil was used as the counter-electrode. The distance between the two electrodes was maintained at 2 cm. All experiments were conducted at about 25 °C. After anodization, samples were washed with deionized (DI) water and ultrasonicated to remove surface debris consisting of precipitate that fell out of solution onto the sample. The nanotube array morphology was imaged using a field emission scanning electron microscope (FESEM, Hitachi S-4700). The nanotubes were then annealed in ambient oxygen at 450 °C for 3 h.

Acknowledgment. The authors thank the Multi-Scale Technologies Institute, NSF-DMR Grant 0820884, the Applied Chemical and Morphological Analysis Laboratory, and Michigan Technological University for providing TEM support to conduct this research.

REFERENCES AND NOTES

1. Mor, G. K.; Varghese, O. K.; Paulose, M.; Grimes, C. A. Fabrication of Tapered, Conical-Shaped Titania Nanotubes. *J. Mater. Res.* **2003**, *18*, 2588–2593.
2. Varghese, O. K.; Gong, D.; Paulose, M.; Ong, K. G.; Grimes, C. A. Hydrogen Sensing Using Titania Nanotubes. *Sens., Actuators B* **2003**, *93*, 338–344.
3. Varghese, O. K.; Gong, D.; Paulose, M.; Ong, K. G.; Dickey, E. C.; Grimes, C. A. Extreme Changes in the Electrical Resistance of Titania Nanotubes with Hydrogen Exposure. *Adv. Mater.* **2003**, *15*, 624–627.
4. Mor, G. K.; Shankar, K.; Paulose, M.; Varghese, O. K.; Grimes, C. A. Enhanced Photocleavage of Water Using Titania Nanotube Arrays. *Nano Lett.* **2005**, *5*, 191–195.
5. Gong, D.; Grimes, C. A.; Varghese, O. K.; Hu, W.; Singh, R. S.; Chen, Z.; Dickey, E. C. Titanium Oxide Nanotube Arrays Prepared by Anodic Oxidation. *J. Mater. Res.* **2001**, *16*, 3331–3334.
6. Paulose, M.; Mor, G. K.; Varghese, O. K.; Shankar, K.; Grimes, C. A. Visible Light Photoelectrochemical and Water-Photoelectrolysis Properties of Titania Nanotube Arrays. *J. Photochem. Photobiol.* **2006**, *178*, 8–15.

7. Varghese, O. K.; Paulose, M.; Shankar, K.; Mor, G. K.; Grimes, C. A. Water-Photolysis Properties of Micron-Length Highly-Ordered Titania Nanotube-Arrays. *J. Nanosci. Nanotechnol.* **2005**, *5*, 1158–1165.
8. Albu, S. P.; Ghicov, A.; Macak, J. M.; Hahn, R.; Schmuki, P. Self-Organized, Free-Standing TiO_2 Nanotube Membrane for Flow-Through Photocatalytic Applications. *Nano Lett.* **2007**, *7*, 1286–1289.
9. Parkhutik, V. P.; Shershulsky, V. I. Theoretical Modelling of Porous Oxide Growth on Aluminium. *J. Phys. D: Appl. Phys.* **1992**, *25*, 1258–1263.
10. Shobha, T.; Sarma, C. S. N.; Sastry, K. S.; Anjaneyulu, C. H. Anodization of Hafnium in Phosphate Baths: Radio Tracer Studies. *Bull. Electrochem.* **2001**, *17*, 519–523.
11. Lu, Q.; Hashimoto, T.; Skeldon, P.; Thompson, G. E.; Habazaki, H.; Shimizu, K. Nanoporous Anodic Niobium Oxide Formed in Phosphate/Glycerol Electrolyte. *Electrochem. Solid-State Lett.* **2005**, *8*, B17–B19.
12. Mor, G. K.; Varghese, O. K.; Paulose, M.; Shankar, K.; Grimes, C. A. A Review on Highly Ordered, Vertically Oriented TiO_2 Nanotube Arrays: Fabrication, Material Properties, and Solar Energy Applications. *Sol. Energy Mater. Sol. Cells.* **2006**, *90*, 2011–2075.
13. Crawford, G. A.; Chawla, A. N.; Das, K.; Bose, S.; Bandyopadhyay, A. Microstructure and Deformation Behavior of Bioactive TiO_2 Coatings. *Acta Biomater.* **2007**, *3*, 359–367.
14. Shan, Z. W.; Mishra, R. K.; Syed Asif, S. A.; Warren, O. L.; Chrzan, D. C.; Minor, A. M. Mechanical Annealing and Source-Limited Deformation in Submicrometre-Diameter Ni Crystals. *Nat. Mater.* **2008**, *7*, 115–119.
15. Shan, Z. W.; Adesso, G.; Cabot, A.; Sherburne, M. P.; Syed Asif, S. A.; Warren, O. L.; Chrzan, D. C.; Minor, A. M.; Alivisatos, A. P. Ultrahigh Stress and Strain In Hierarchically Structured Hollow Nanoparticles. *Nat. Mater.* **2008**, *7*, 947–952.
16. Kuzumaki, T.; Yoshitaka, M. Nanoscale Mechanics of Carbon Nanotube Evaluated by Nanoprobe Manipulation in Transmission Electron Microscope. *J. Appl. Phys.* **2006**, *45*, 364–368.
17. Huang, J. Y.; Chen, S.; Ren, Z. F.; Wang, Z. Q.; Wang, D. Z.; Vaziri, M.; Suo, Z.; Chen, G.; Dresselhaus, M. S. Kink Formation and Motion in Carbon Nanotubes at High Temperatures. *Phys. Rev. Lett.* **2006**, *97*, 075501–4.
18. Golberg, D.; Costa, P. M. F. J.; Lourie, O.; Mitome, M.; Bai, X.; Kurashima, K.; Zhi, C.; Tang, C.; Bando, Y. Direct Force Measurements and Kinking under Elastic Deformation of Individual Multiwalled Boron Nitride Nanotubes. *Nano Lett.* **2007**, *7*, 2146–2151.
19. Ertsa, D.; Lohmusb, A.; Lohmusb, R.; Olinc, H.; Pokropivnyd, A. V.; Ryenc, L.; Svensson, K. Force Interactions and Adhesion of Gold Contacts Using a Combined Atomic Force Microscope and Transmission Electron Microscope. *Appl. Surf. Sci.* **2002**, *188*, 460–466.
20. Bai, X.; Golberg, D.; Bando, Y.; Zhi, C.; Tang, C.; Mitome, M.; Kurashima, K. Deformation-Driven Electrical Transport of Individual Boron Nitride Nanotubes. *Nano Lett.* **2007**, *7*, 633–638.
21. Yakobson, B. I.; Campbell, M. P.; Brabec, C. J.; Bernholc, J. High Strain Rate Fracture and C-Chain Unraveling in Carbon Nanotubes. *Comput. Mater. Sci.* **1997**, *8*, 341–348.
22. Yu, M. F.; Lourie, O.; Dyer, M. J.; Moloni, K.; Kelly, T. F.; Ruoff, R. S. Strength and Breaking Mechanism of Multiwalled Carbon Nanotubes Under Tensile Load. *Science* **2000**, *287*, 637–640.
23. Ding, W.; Calabri, L.; Kohlhaas, K. M.; Chen, X.; Dikin, D. A.; Ruoff, R. S. Modulus, Fracture Strength, and Brittle *vs* Plastic Response of the Outer Shell of Arc-Grown Multi-Walled Carbon Nanotubes. *Exp. Mech.* **2007**, *47*, 25–36.
24. Lu, S. N.; Guo, Z. Y.; Ding, W. Q.; Dikin, D. A.; Lee, J.; Ruoff, R. S. *In Situ* Mechanical Testing of Templated Carbon Nanotubes. *Rev. Sci. Instrum.* **2006**, *77*, 125101.
25. Ding, W. Q.; Calabri, L.; Chen, X. Q.; Kolhaas, K. M.; Ruoff, R. S. Mechanics of Crystalline Boron Nanowires. *Compos. Sci. Technol.* **2006**, *66*, 1109–1121.